NANO LETTERS

Letter

pubs.acs.org/NanoLett

Large-Scale Sublattice Asymmetry in Pure and Boron-Doped Graphene

Dmitry Yu. Usachov,[*,†] Alexander V. Fedorov,[†,‡,§] Oleg Yu. Vilkov,[†] Anatoly E. Petukhov,[†] Artem G. Rybkin,[†] Arthur Ernst,[∥] Mikhail M. Otrokov,[⊥,#,†] Evgueni V. Chulkov,[†,⊥,#] Ilya I. Ogorodnikov,[▽] Mikhail V. Kuznetsov,[▽] Lada V. Yashina,[○] Elmar Yu. Kataev,[○] Anna V. Erofeevskaya,[†] Vladimir Yu. Voroshnin,[†] Vera K. Adamchuk,[†] Clemens Laubschat,[◆] and Denis V. Vyalikh[†,⊥,◆,¶]

[†]St. Petersburg State University, 7/9 Universitetskaya nab, St. Petersburg, 199034, Russia

[‡]II Physikalisches Institut, Universität zu Köln, Zülpicher Strasse 77, 50937 Köln, Germany

[§]IFW Dresden, P.O. Box 270116, D-01171 Dresden, Germany

[∥]Max-Planck-Institut für Mikrostrukturphysik, Weinberg 2, D-06120 Halle, Germany

[⊥]Donostia International Physics Center (DIPC), Departamento de Fisica de Materiales and CFM-MPC UPV/EHU, 20080 San Sebastian, Spain

[#]Tomsk State University, Lenina Avenue, 36, 634050 Tomsk, Russia

[▽]Institute of Solid State Chemistry of the Ural Branch of the Russian Academy of Sciences, Pervomayskaya Street 91, 620990 Ekaterinburg, Russia

[○]M.V. Lomonosov Moscow State University, Leniskie Gory 1/3 199991 Moscow, Russia

[◆]Institute of Solid State Physics, Dresden University of Technology, 01062 Dresden, Germany

[¶]IKERBASQUE, Basque Foundation for Science, 48011 Bilbao, Spain

Supporting Information

ABSTRACT: The implementation of future graphene-based electronics is essentially restricted by the absence of a band gap in the electronic structure of graphene. Options of how to create a band gap in a reproducible and processing compatible manner are very limited at the moment. A promising approach for the graphene band gap engineering is to introduce a large-scale sublattice asymmetry. Using photoelectron diffraction and spectroscopy we have demonstrated a selective incorporation of boron impurities into only one of the two graphene sublattices. We have shown that in the well-oriented graphene on the Co(0001) surface the carbon atoms occupy two nonequivalent positions with respect to the Co lattice, namely top and hollow sites. Boron impurities embedded into the graphene lattice preferably occupy the hollow sites due to a site-specific interaction with the Co pattern. Our theoretical calculations predict that such boron-doped graphene possesses a band gap that can be precisely controlled by the dopant concentration. B-graphene with doping asymmetry is, thus, a novel material, which is worth considering as a good candidate for electronic applications.

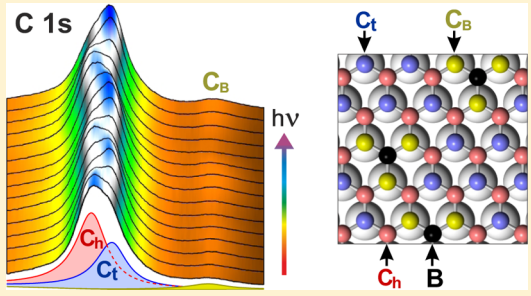

KEYWORDS: *Graphene, boron, doping, sublattice asymmetry, electronic structure, photoemission spectroscopy*

Among astonishing properties of graphene a high mobility of charge carriers has placed this material into the focus of intensive research efforts, aimed at developing high-speed graphene-based electronic devices.[1] The first device of this family, a graphene field-effect transistor[2] (GFET), remains a promising candidate for applications in flexible electronic circuits.[3] An essential handicap that limits the performance of planar GFETs is the absence of a band gap in the graphene electronic structure. The gap is necessary to reach a high on/off current ratio. In the recent past, several approaches have been developed for opening and controlling the gap. These methods include adsorption of atoms and molecules,[4,5] dimensional narrowing,[6] application of a strong electric field,[7] and so forth. However, the method providing sufficiently stable systems with reproducible intrinsic band gap is still required. A promising solution proposed theoretically is known as sublattice asymmetry of doping or unbalanced sublattice doping. The key point here is the incorporation of impurities into only one of the two available sublattices of graphene.[8,9] According to the theory, when the impurities randomly substitute the carbon atoms in two sublattices, then the resulting graphene-based

Received: May 3, 2016
Published: June 1, 2016

DOI: 10.1021/acs.nanolett.6b01795
Nano Lett. 2016, 16, 4535−4543

material still remains gapless. However, when the foreign atoms become randomly embedded only in one graphene sublattice, the resulting system possesses a notable band gap[10] improving the transport properties of conventional GFETs.[9]

Experimental observation of the discussed unbalanced sublattice doping is quite elusive.[8] Doping asymmetry was detected with scanning tunneling microscopy (STM) in nitrogen-doped graphene, grown on a Cu(111) substrate.[11] It was proposed that a possible mechanism responsible for breaking of the sublattice symmetry is related to oscillations in the local density of states driven by the impurities.[12] Such oscillations may be of importance in the case of quasi-freestanding N-graphene that weakly interacts with the copper substrate, when the dopant concentration does not exceed ~1 atom %.[12] A study of boron-doped graphene (B-graphene) on Cu(111) revealed no doping asymmetry.[13] It was proposed that stronger interaction of copper with boron, compared to nitrogen, prevents the symmetry breaking.[13] However, for other substrates the situation may be different. In particular, we have recently shown[14] that B-graphene on a Ni(111) substrate, where the metal strongly interacts with the boron atoms, exhibits the doping asymmetry at the boron concentration of ~4 atom %. In this case, a good matching between the graphene and the substrate lattices plays a crucial role. While in the graphene/Cu(111) system the lattice parameters mismatch is quite significant and equals 3.7%, the difference is only 1.1% in the case of Ni(111) substrate, which ensures excellent matching of the lattices. Upon this condition, strong interaction with the substrate becomes a driving force for the asymmetrical doping.

Our approach is illustrated in Figure 1. When doped graphene is synthesized on a crystal face with hexagonal

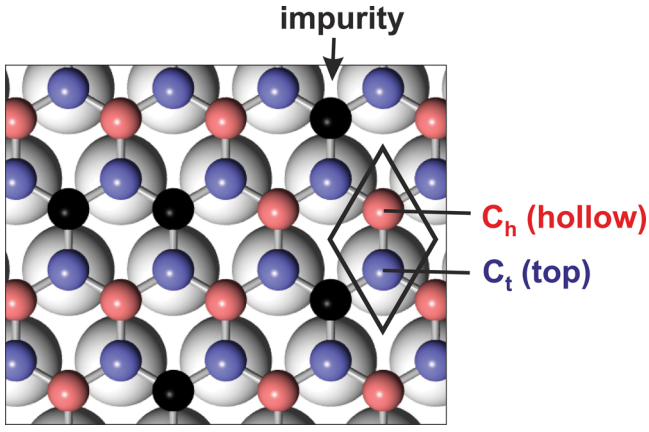

Figure 1. Concept of using a single-crystalline lattice-matched substrate as a pattern for unbalanced sublattice doping of graphene. In the top-hollow interface structure impurities may occupy sites in one sublattice.

structure and well-matched lattice constant, a strong symmetry breaking may occur. This happens when one sublattice, marked as C_t, is adsorbed on top of the substrate atoms, while the other sublattice C_h occupies the hollow sites. In this case, the impurities may have strongly different probabilities for embedding in these sublattices due to a site-specific interaction with the substrate. The most promising candidates for realization of such a scenario are the Ni(111) and Co(0001) surfaces that have lattice mismatch with graphene less than 2%. However, reliable identification of the doping asymmetry is a quite challenging task. Until now, the only experimental technique used for such observations was STM,[11,13,14] which is a very local method. The scale of atomically resolved images is usually below 100 nm and acquisition of large high-quality images is hard and time-consuming. Thus, it is rather nontrivial to prove the existence of the doping asymmetry at the macroscopic scale with STM. Here, we demonstrate an efficient approach for large-scale observation of the doping asymmetry by means of photoemission techniques.

Prior to the discussion of the results, let us consider the structure of undoped graphene on the Ni(111) and Co(0001) surfaces. Numerous attempts to determine the structure of the graphene/Ni(111) interface have been made over the last few decades.[15−19] Theoretically, there are three favorable adsorption geometries with a minor energy difference:[20] two asymmetric structures with carbon atoms positioned in top sites and in hollow (either face-centered cubic or hexagonal close-packed) sites, namely top-fcc and top-hcp structures, and a bridge-top configuration in which the carbon sublattices occupy symmetric positions with respect to the substrate surface atomic layer. Early experimental studies with surface-extended energy-loss fine structure (SEELFS) spectroscopy have suggested the fcc-hcp structure.[15] Further analysis with low-energy electron diffraction[16] (LEED) and ion scattering spectroscopy[17] pointed to the asymmetric top-fcc geometry. Recent LEED studies indicated that in different samples the structure can be either top-fcc or bridge-top, or a mixture of both.[18] Finally, STM studies revealed a coexistence of the top-fcc, top-hcp, and bridge-top structures in one sample.[19] These results indicate that the interface structure is not well-defined and must be carefully determined for each specific graphene/Ni(111) sample.

The early studies of the graphene/Co(0001) system showed that graphene is formed by randomly oriented domains sticked to the metallic substrate.[21,22] However, it was recently shown that under certain conditions well-oriented graphene can be grown.[23,24] But the properties of such an interface, and particularly its geometry, remain poorly explored. In the present work, we unveil the structural properties of the graphene/Co(0001) interface and show that the cobalt substrate is very well suitable for large-scale unbalanced doping of graphene with substitutional boron impurities.

The Structure of Graphene on the Co(0001) Surface. It is well-known that the line shape of the C 1s photoemission spectra may efficiently reflect the structure of the graphene/metal interface.[25] Therefore, we begin with an analysis of the X-ray photoelectron spectroscopy (XPS) spectra obtained for two single-layer graphene samples, which were synthesized by CVD on the Co(0001) surface (see Methods for details) at two different temperatures, resulting in contrasting properties of the interface. Figure 2 shows the LEED patterns, crystal structure models, STM images, and the XPS spectra of the two graphene/Co(0001) systems, synthesized at 550 °C (Figure 2a) and 650 °C (Figure 2b). As evidenced by the LEED pattern, the graphene grown at lower temperature is polycrystalline and consists of multiple misoriented domains. The STM image of misoriented graphene domain demonstrates well-known periodic moiré pattern, which originates from the lattice misfit. In this case, carbon atoms are located in numerous different positions with respect to the cobalt surface lattice. Each position is characterized by its own binding energy of the C 1s line. As a result, the corresponding XPS spectrum consists of a single broadened peak formed as a superposition

DOI: 10.1021/acs.nanolett.6b01795
Nano Lett. 2016, 16, 4535−4543

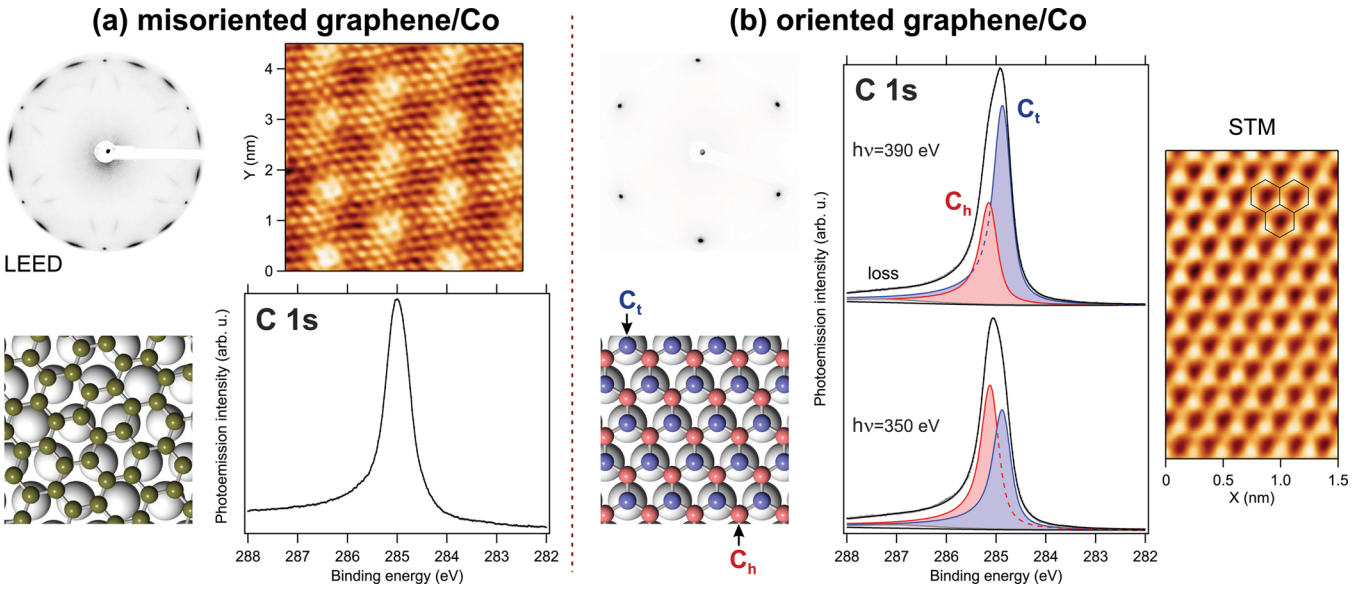

Figure 2. LEED patterns, crystal structure models, XPS spectra, and STM images of (a) misoriented and (b) oriented graphene on Co(0001). The XPS spectrum of misoriented graphene/Co was acquired using a photon energy of 320 eV, although it looks similar at any other excitation energy. The LEED patterns were obtained with an electron beam energy of 70 eV. The STM images were obtained using a bias voltage of 5 mV at a constant current of 2 nA.

of signals from each carbon atom. The measured full width at half-maximum of this peak equals ~0.6 eV. The graphene grown at higher temperature appears well oriented in accordance with our recent study.[24] Its LEED pattern shows a perfect hexagon, which could be expected for a single crystal. The corresponding STM image exhibits no moiré pattern, thus indicating a perfect matching of the graphene and Co lattices. The C 1s XPS spectrum of such oriented graphene has a complex shape, which cannot be described with a single peak. However, it can be nicely decomposed in two components, C_t and C_h, with identical shapes but different binding energies (BE) of 284.90 and 285.17 eV, respectively, and with the width of ~0.4 eV. This can be readily explained by the two preferred positions of the carbon atoms. On the basis of the STM data, which clearly demonstrate asymmetry between the graphene sublattices, it is natural to relate different peaks to the two sublattices. Particularly, the component C_t corresponds to the graphene sublattice located on top of the cobalt atoms, while C_h originates from the second sublattice located above the hollow sites of the Co(0001) surface in accordance with the model structure in Figure 2b. Such interpretation is consistent with our density functional theory (DFT) calculations (see Table 1), which predict significant splitting of the C 1s peak in the top-hollow configurations, namely top-fcc and top-hcp.

Another essential feature of the C 1s spectrum of the oriented graphene is the strong dependence of its shape on the photon energy ($h\nu$). As can be seen in Figure 2b, at the photon energy of 390 eV the C_t peak is nearly twice as high as the C_h peak, while at $h\nu$ = 350 eV the C_h peak becomes more intensive than the C_t. To explore further this interesting observation, we followed the evolution of the spectral structure of the C 1s line by varying the photon energy in a wide range. The respective photoemission spectra are partially shown in Figure 3a. Obviously, the energy positions of the spectral intensity maxima exhibit nonmonotonic variations, which can be explained by the changes in the relative intensities of the C_t and C_h peaks. These intensity oscillations undoubtedly originate from the well-known photoelectron diffraction

Table 1. C 1s Core Level Shifts of Pure and B-Doped Graphene on Co(0001), Estimated with DFT in Initial State Approximation[a]

structure	C_h, eV	C_t, eV	C_B, eV[b]
top-fcc, pure	+0.35	0	
top-hcp, pure	+0.46	+0.09	
bridge-top, pure	+0.15	+0.15	
top-fcc, 3.1 atom % B	+0.24 to 0[c]	−0.13 to −0.28[c]	−1.45

[a]The shifts are given relative to the C_t sublattice in pure graphene/Co with top-fcc structure. [b]C_B indicates carbon atoms bonded with one B atom and two C atoms. [c]The C 1s energy in B-graphene depends on the relative positions of the C and B atoms.

(PED) phenomena. Qualitatively, the observation of PED itself points to a good crystallinity of the interface. Quantitatively, it contains extensive information on the crystal structure of the near-surface atomic layers. Thus, in order to determine the structure of the graphene/Co(0001) interface, all C 1s spectra were accurately decomposed in C_t and C_h components and the C_t/C_h intensity ratio was evaluated for each photon energy. The obtained values, shown as red curves in Figure 3b, were compared with the results of the PED simulations performed for three different interface structures: top-fcc, top-hcp, and bridge-top. These configurations were chosen as the most probable according to the theoretical and experimental studies of the allied graphene/Ni(111) system.[19,20] Comparison of the experimental results and the modeling brings us to the conclusion that the top-fcc structure provides the best fit to the experiment. Only the local minimum predicted by the simulation at $h\nu$ = 380 eV is not resolved in the experiment. A possible reason for such a discrepancy will be discussed hereinafter. In the case of the top-hcp configuration the quantitative agreement between the experiment and the simulation is worse, however, it is still relatively good at the qualitative level. This is explained by the fact that due to the high surface sensitivity of XPS the major contribution to the PED is determined by location of the surface Co atoms relative

DOI: 10.1021/acs.nanolett.6b01795
Nano Lett. 2016, 16, 4535−4543

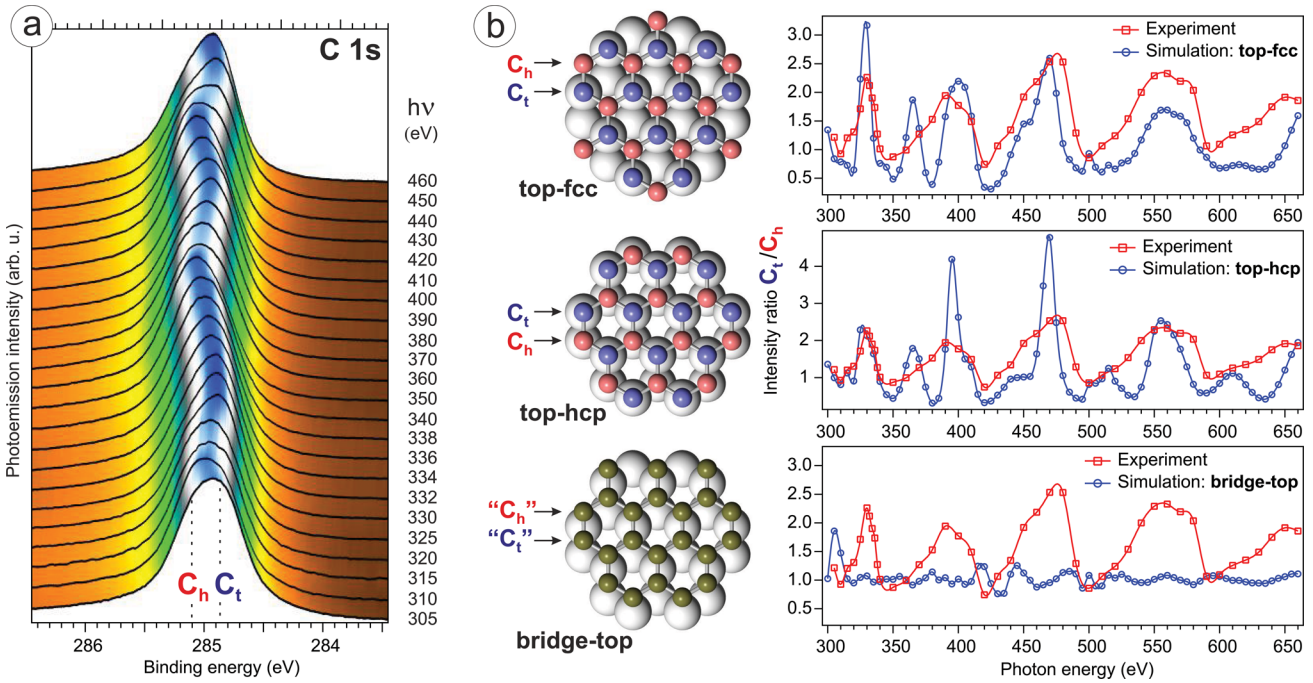

Figure 3. (a) XPS spectra of graphene/Co(0001) system as a function of photon energy. (b) Calculated and measured intensity ratio C_t/C_h for different interface structures.

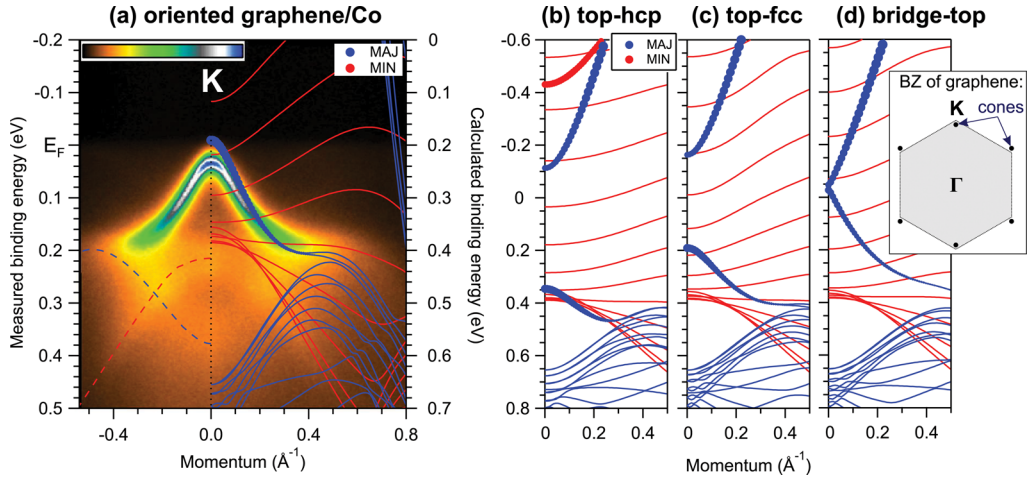

Figure 4. (a) ARPES of an oriented graphene/Co(0001) sample, measured using photon energy of 36 eV at a temperature of 40 K, compared with the calculated band structure in top-fcc configuration. Dashed lines indicate measured edges of bulk Co 3d bands. (b–d) Calculated spin-dependent bands of graphene/Co(0001) systems with different interface structures. The labels MAJ and MIN indicate majority and minority spins. Line thickness is proportional to the contribution of carbon to the wave function. All calculated and measured data are presented along the path in **k**-space, which is perpendicular to ΓK direction of the graphene BZ and passes through the Dirac cone apex.

to graphene. This location is similar in both top-fcc and top-hcp structures. The difference in PED is determined by the second and deeper lying Co layers. In the case of the bridge-top structure no pronounced PED effects are expected in the C_t/C_h ratio, because C atoms are located symmetrically relative to the topmost Co atoms. Thus, we can conclude that the top-fcc configuration is the preferred structure of oriented graphene on the Co(0001) surface.

This conclusion is further supported by the analysis of the experimental results obtained with angle-resolved photoemission spectroscopy (ARPES). Recently, we have shown that in the electronic structure of oriented graphene on Co(0001) a spin-polarized interface state is formed due to hybridization of the graphene π-states with the Co 3d states.[24] This hybrid state has conical dispersion in a tiny energy range near the Fermi level, therefore we call it a mini Dirac cone. The minicone is not observed in the case of misoriented graphene on Co, thus, it is very sensitive to the interface geometry. Figure 4a presents high-resolution ARPES data measured at a temperature of 40 K near the **K**-point of the Brillouin zone (BZ). The sharp intensive band is a mini Dirac cone, while weak features marked with dashed lines originate from the edges of projected bulk Co 3d bands with high density of states. In order to determine the interface structure, we compared the measured dispersion with electronic bands derived from the DFT calculations. Figure 4b–d shows dispersions calculated for different interface structures. Obviously, the minicone states look quite similar in the top-fcc and top-hcp configurations due

DOI: 10.1021/acs.nanolett.6b01795
Nano Lett. 2016, 16, 4535–4543

to nearly identical relative positions of carbon and the topmost cobalt atoms. In both structures, the two graphene sublattices have nonequivalent positions with respect to the surface Co atoms; therefore the substrate breaks the sublattice symmetry. This results in the opening of a significant local band gap in the Dirac cone. In the bridge-top structure the first Co layer is symmetrically positioned relative to the graphene sublattices, and the symmetry is broken by the interaction with the more distant second Co layer, which weakly interacts with graphene. For this reason the gap almost vanishes. Also it should be noted that the bridge-top structure has no 3-fold symmetry axis, therefore the Dirac cones appear slightly shifted from their positions in the BZ of freestanding graphene, as it is shown in the inset of Figure 4d. While looking into the low-temperature ARPES data one can clearly see that the minicone apex has parabolic dispersion, which excludes the bridge-top structure. The effective mass in the cone apex equals ~0.6 of the free electron mass. Comparison of the calculated and experimental bands leads to the conclusion that the top-fcc configuration agrees better with the experimental data. The agreement becomes more obvious after shifting the calculated bands by 0.2 eV, as it is done in the right part of Figure 4a. This value does not exceed the range of typical discrepancies between the calculated and measured energies. Nevertheless, the top-hcp structure also agrees with the experiment at a qualitative level and therefore cannot be reliably excluded based on the ARPES data only.

Summing up the presented discussion we can affirm the presence of a strong sublattice asymmetry in the studied oriented graphene on the Co(0001) surface. The existence of the asymmetry can be easily detected with XPS as the presence of diffraction effects. Here it should be noted that in our experiment the area probed with XPS has the size of about 90 μm, while the size of the graphene/Co sample is nearly 1 cm. When moving the X-ray spot to various regions on the sample surface we have always observed identical XPS spectra with PED effects. Thus, we can say that asymmetry is present on a large scale, implying that it is observed at any microscopic place of the large sample surface. On the other hand, it is quite obvious that the two graphene sublattices A and B are absolutely equivalent, and therefore in one place of the cobalt surface the sublattice A may grow in the top position, while at another place the sublattice B can be the top one. Thus, the interface may consist of two types of domains. The size of these domains determines the local length scale of sublattice asymmetry. This scale cannot be derived from the photoelectron spectroscopy or diffraction data, therefore the STM must be used. A reasonably large STM image of the oriented graphene/Co system is presented in Figure S1 of the Supporting Information. It demonstrates sublattice asymmetry and the length scale of asymmetry extends over range of ~20 nm. This allows on to conclude that the local length scale of sublattice asymmetry is at least a few dozens of nanometers. Undoubtedly, this length scale is large enough for the formation of a well-defined electronic band structure.

It is worth noting that photoelectron diffraction effects are expected in XPS spectra of the allied graphene/Ni(111) system in the case of a dominating top-fcc or top-hcp structure. However, we have studied dozens of graphene/Ni(111) samples synthesized at various temperatures and have never observed any diffraction effects in the C 1s XPS spectral shape. This may indicate either a preferred bridge-top structure or the absence of precise lattice matching. Better ordering of the interface in the case of the graphene/Co(0001) may be explained by a higher adsorption energy of graphene on Co in comparison with Ni.[26] Thus, the Co(0001) substrate seems to be the most promising template for synthesis of doped graphene with preferential embedding of impurities in one sublattice on a large scale. Here we demonstrate this by the example of boron-doped graphene.

Doping Asymmetry in B-Graphene on the Co(0001) Surface. Let us now turn to the discussion of B-graphene, which was synthesized on the Co(0001) surface with the CVD method using propylene and carborane at a temperature of 620 °C, as described in Methods. According to our previous study,[14] the concentration of boron in graphene may reach 19 atom %, however, at such a high doping level the crystal structure of B-graphene is strongly distorted and no sublattice asymmetry of doping can be expected. Thus, we have reduced the exposure to carborane during the synthesis in order to limit the boron content to a few atom %. As a result, a sample with 2.4 atom % of boron was synthesized. The LEED pattern, the crystal structure model, and the C 1s XPS spectra of the B-graphene/Co(0001) system are shown in Figure 5. It is worth noting that the synthesis of undoped graphene at the same temperature of 620 °C led to formation of misoriented graphene with the same type of LEED pattern as shown in Figure 2a, whereas the LEED pattern of B-graphene is a perfect hexagon, indicating strict orientation of its honeycomb lattice. This fact allows us to assume that at low concentration boron has positive influence on the graphene orientation.

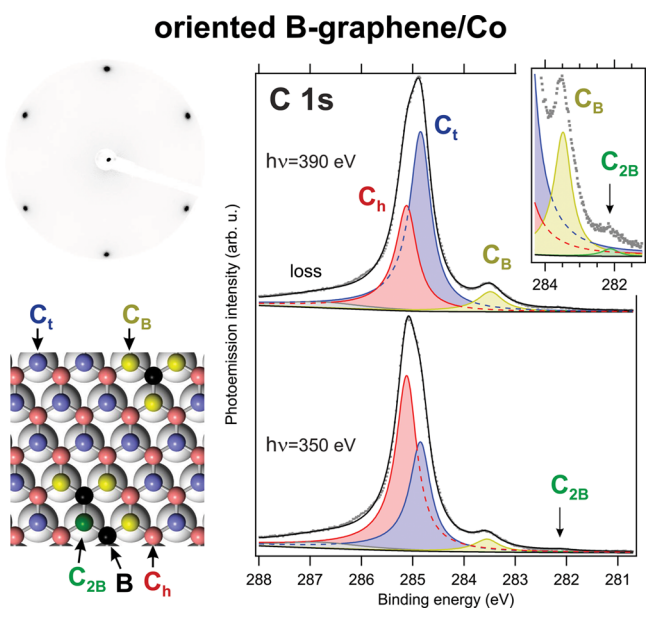

Figure 5. LEED pattern, crystal structure model, and XPS spectra of the B-graphene/Co(0001) system with 2.4 atom % of boron impurities. The LEED pattern was obtained with an electron beam energy of 70 eV.

The C 1s XPS spectra of B-graphene/Co(0001) have a complex shape, which can be described by the presence of at least four components. Similarly to the case of pure oriented graphene the two most intensive components C_t and C_h can be identified as those of carbon atoms located in different sublattices and having no bonds with B atoms. The relative intensities of these components exhibit a strong dependence on the photon energy due to the PED effects as discussed above.

DOI: 10.1021/acs.nanolett.6b01795
Nano Lett. 2016, 16, 4535−4543

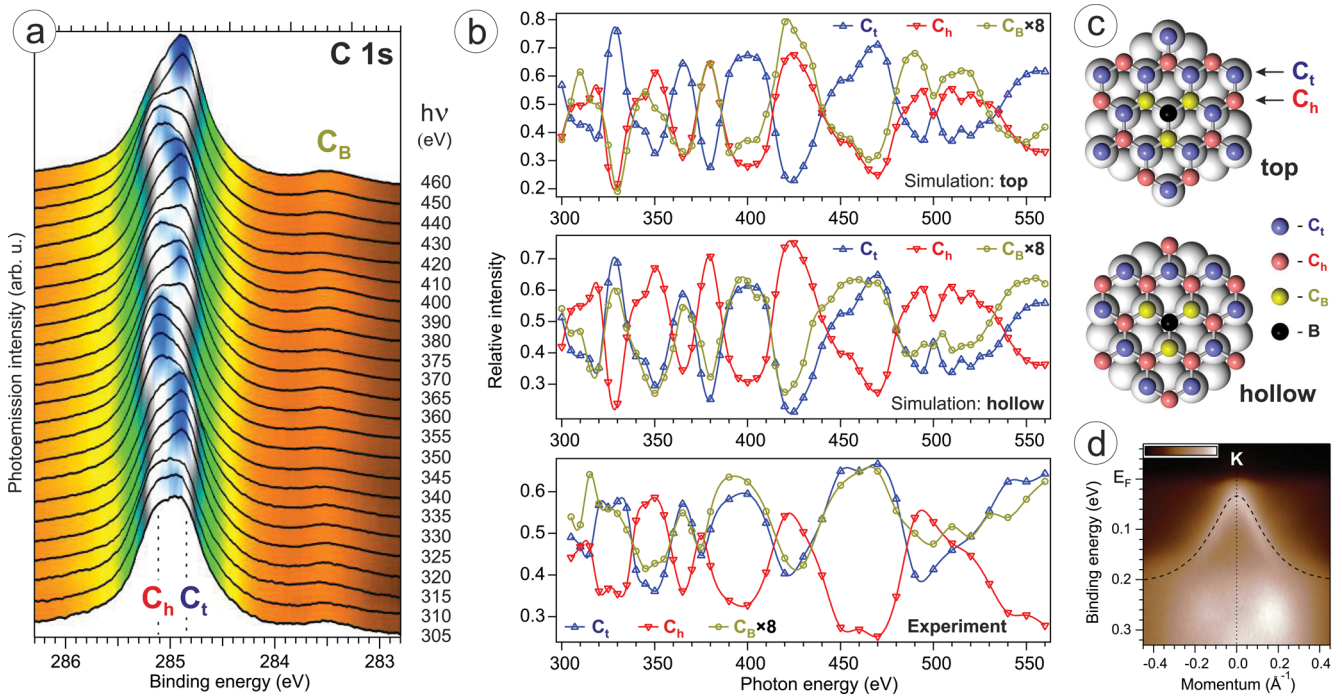

Figure 6. (a) XPS spectra of B-graphene/Co(0001) at a boron concentration of 2.4 atom % as a function of photon energy. (b) Calculated and measured relative intensities of the peaks C_t, C_h, and C_B for different locations of the boron atoms, shown in the panel (c). (d) ARPES image, measured with He I radiation ($h\nu$ = 21.2 eV). Dashed line indicates measured minicone dispersion of undoped graphene/Co. The direction of measurements is the same as in Figure 4a.

The other two components C_B and C_{2B} have significantly differing binding energies, indicating different local environments of C atoms. As it was well-founded in previous works,[14,27] the peak C_B at the BE of 283.5 eV corresponds to carbon atoms bonded with two C atoms and one B atom (BC_2 environment). Its chemical shift relative to the peak C_t equals −1.35 eV, which is in a perfect agreement with the calculated value, presented in the Table 1. The peak C_{2B} at the BE of 282.1 eV corresponds to carbon atoms that form bonds with two B atoms and one C atom[14,27] (B_2C environment). This peak is hardly detectable, so it will be neglected in our further discussion. The B 1s XPS spectra can be reliably described with only one component; therefore these spectra are not presented.

On the basis of the PED effects one can easily identify the structure of the B-graphene/Co(0001) interface. The measured dependence of the C 1s XPS spectra on the photon energy is presented in Figure 6a. Interestingly, the C_t and C_h peaks appear sharper than for the pure graphene as shown in Figure 3a, although the measured energy separation of these components is identical and equals 0.27 eV. This observation supports the assumption that a small amount of boron improves the matching between graphene and Co(0001) lattices. Assuming that B-graphene has the same top-fcc adsorption geometry as pure graphene/Co, we calculated the relative intensities of the peaks C_t, C_h, and C_B as a function of $h\nu$ for the two possible locations of the impurities: top and hollow. The boron concentration was set to 2.4 atom % to simulate the experiment. The results are shown in the upper and middle parts of Figure 6b. It follows from the simulation that the intensity of the peak C_B must strongly correlate with the intensity of C_t for the hollow site location of the B atom and with that of C_h for boron incorporated into the top site. The lower part of Figure 6b demonstrates the measured intensities as obtained by decomposition of the XPS spectra. Obviously, the C_B intensity follows the C_t curve, indicating that the C atoms bonded with boron are located in the top sublattice. Thus, the impurities preferably occupy the hollow positions. The existence of preferred boron position is consistent with the observation of a single peak in the B 1s XPS spectra.

It should be emphasized that there is a good matching between the calculated and the measured oscillations of the C_t and C_h intensities in the case of B-graphene. The local minimum of the C_t intensity at 380 eV was not resolved in the XPS/PED data of undoped graphene (see Figure 3), however it is clearly visible in Figure 6b. Thus, the B-graphene/Co system demonstrates better agreement with the proposed ideal top-fcc model than the pure graphene/Co. This conclusion once again indicates better matching between the graphene and Co(0001) lattices in the presence of a small amount of boron. In order to explain this phenomenon, we carried out DFT calculations of the B-graphene/Co system in the top-fcc configuration (see Methods for simulation details). As a result, it was found that B atoms strongly prefer to substitute carbon atoms located in the fcc (hollow) sites of the Co(0001) substrate in agreement with the PED data analysis. Moreover, the energy gain with respect to the case when a B atom is incorporated into the top site equals 0.377 eV. This energy is much higher than the binding energy of each graphene C atom with the Co(0001) surface (~0.16 eV).[26] Thus, graphene is forced to match the substrate lattice in the vicinity of impurities.

The range of boron concentrations at which the splitting of the main C 1s peak in C_t and C_h components could be observed is probably limited to a few atom %. This is evidenced by our previous XPS study of the B-graphene/Co(0001) system with 4.5 atom % of boron, where no splitting was detected.[14] Our calculations predict that at the presence of impurities both C_t and C_h peaks must be broadened due to the scattering of their BEs (see Table 1). This effect is intensified at a higher doping

DOI: 10.1021/acs.nanolett.6b01795
Nano Lett. 2016, 16, 4535−4543

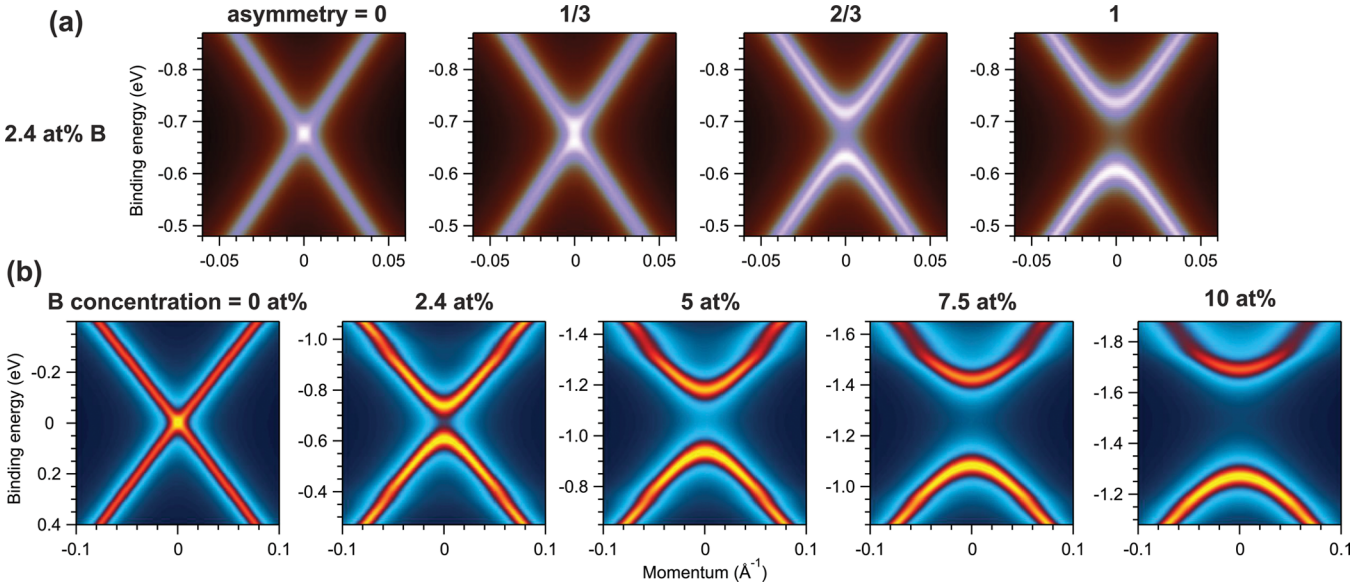

Figure 7. Calculated Dirac cone of a B-doped freestanding graphene: (a) as a function of the doping asymmetry $|n_1 - n_2|/(n_1 + n_2)$ at the fixed boron concentration of 2.4 atom %, and (b) as a function of B concentration at the maximal asymmetry (all impurities located in one sublattice). The path in the **k**-space, is perpendicular to ΓK direction of the BZ.

level and may hinder the observation of the splitting. Nevertheless, the PED effects should not vanish if the interface structure retains high quality. Thus, we believe that further PED studies of B-graphene at different doping levels will allow determining precisely the maximal boron concentration that still ensures the large-scale doping asymmetry.

For comprehensiveness of the presented study let us consider the ARPES data of B-graphene/Co, shown in Figure 6d. Obviously, the minicone can be well seen near the Fermi level, similarly to the pure graphene/Co(0001) system. The wave function of the minicone state is localized on the sublattice C_h, which contains randomly distributed boron impurities. Violation of the periodicity leads to electron scattering that results in notable broadening of the spectral function for the interface state, however the energy position remains unaffected at low boron concentration. At the very high dopant concentration of 15 atom %, the minicone state cannot be seen any more in the ARPES spectral pattern, according to our previous study.[14] Thus, the intensity of the interface state is quite sensitive to the presence of impurities. This is in contrast with the behavior of the π-band in the graphene/Co and graphene/Ni systems, where the π-states undergo energy shift toward the Fermi level upon doping with boron.[14,27]

Band Gap in Freestanding B-Graphene. In order to investigate possible B-graphene applications in electronic devices it is necessary to estimate the influence of boron impurities on the electronic structure of graphene once it is removed from the metal substrate and transferred onto an insulator. For this purpose, we have carried out ab initio band structure calculations for a freestanding B-graphene (see Methods for the simulation details). Figure 7a illustrates the influence of the doping asymmetry on the Dirac cone of B-graphene. In the case when B impurities are randomly distributed in both sublattices with equal concentrations the A−B symmetry is preserved, therefore the conduction band meets the valence band in the Dirac point (see the first panel in Figure 7a). Thus, the only difference with respect to the undoped graphene case, as shown in the first panel of Figure 7b, is the *p*-type doping of the Dirac cone. The increase of the doping asymmetry (i.e., the disbalance of boron concentrations in two sublattices) immediately leads to the lifting of the 4-fold degeneracy of the Dirac point, that is, to the opening of a band gap. The gap width increases with the doping asymmetry approximately as a linear function. For the boron concentration of 2.4 atom %, as in our experiment, the gap size equals ∼0.13 eV. Further increase of the boron concentration results in a stronger *p*-doping and in a larger gap in the Dirac cone, as it is shown in Figure 7b. At the maximal doping asymmetry, the gap width E_g changes with the B concentration n as $E_g \approx 0.067n^{0.8}$, reaching ∼0.42 eV at n = 10 atom %. Such a dependence is qualitatively similar to the results of a tight-binding simulation for nitrogen-doped graphene.[9] However, in the case of boron doping the predicted gap width is somewhat smaller.

Beside the inversed sign of the charge carriers, one of the differences between the asymmetrical boron and nitrogen doping is an inversed location of the wave functions at the gap edges. In N-graphene, the carriers just below the gap live in the doped sublattice, whereas above the gap the wave function is localized on the undoped (or less doped) sublattice.[9] In B-graphene, the carriers above the gap live in the doped sublattice, whereas the states below the gap belong to the undoped sublattice. Thus, highly asymmetric electronic transport is expected in both N-graphene and B-graphene.

It should be noted that for possible applications of pure or doped graphene grown on a single-crystalline cobalt surface, there is a need for an efficient procedure for graphene transfer onto a semiconducting or insulating substrate. We have found that graphene can be transferred from the Co(0001)/W(110) surface with a bubbling procedure,[28] however the surface of the W crystal becomes rough and needs to be repolished. This problem was successfully overcome by replacing the W(110) substrate with Ir(111). The Ir(111) surface can be easily cleaned from Co remnants after the bubbling transfer and no significant degradation of the surface quality was observed. This

DOI: 10.1021/acs.nanolett.6b01795
Nano Lett. 2016, 16, 4535−4543

allowed one to repeat the synthesis and transfer procedures several times.

In summary, applying photoelectron spectroscopy and analyzing the photoelectron diffraction effects in XPS, we have given a clear evidence for a large-scale sublattice asymmetry in pure and boron-doped graphene grown on the Co(0001) substrate. In the well-oriented graphene/Co(0001) system, one sublattice of carbon is placed above Co atoms, while the second one occupies the hollow sites. This unique property of the interface makes cobalt an ideal substrate to be used as a platform for the synthesis of doped graphene with impurities incorporated in one of the two C-sublattices. This is conclusively demonstrated by the example of the B-graphene/Co(0001) system, in which boron impurities preferably substitute carbon atoms in one sublattice, located above the hollow sites of the metal substrate. The ab initio calculations predict that such asymmetrically doped graphene should have an intrinsic band gap and the width of the gap can be controlled by the dopant concentration. Finally, B-graphene with demonstrated doping asymmetry becomes a novel material, which is worth considering as a good candidate for applications in GFETs and other graphene-based electronics.

Methods. Single-layer pure and boron-doped graphene were synthesized under the ultrahigh vacuum (UHV) conditions by CVD on a crystalline Co(0001) film with a thickness of 10−12 nm, deposited on a clean W(110) surface. The base pressure in the UHV chamber was 2×10^{-10} mbar. The LEED pattern of the Co(0001) film always showed a sharp (1×1) hexagonal pattern, indicating good crystallinity of the metal film. The synthesis of pure graphene was carried out as follows: the substrate was heated up to the synthesis temperature, then propylene (C_3H_6) with a pressure of 10^{-6} mbar was introduced into the vacuum chamber for 15 min. Under these conditions graphene growth starts immediately on the hot metal surface, and the reaction is self-limited to a single layer. After the monolayer formation the growth is stopped as the catalytically active metal surface is passivated with graphene.[29] For the synthesis of boron-doped graphene, the following procedure was used: the substrate was heated up to 620 °C, then during 3 min the sample was exposed to carborane ($C_2B_{10}H_{12}$) vapor with a pressure of 5×10^{-8} mbar. This step determines the amount of boron incorporated in B-graphene.[14] Afterward, propylene was introduced into the chamber at a pressure of 10^{-6} mbar additionally to carborane. After 15 min of the synthesis, the sample was cooled down to room temperature with a rate of ∼1 °C/sec (although the cooling rate is of minor importance).

The synthesis and the XPS/PED measurements were carried out at the Russian−German beamline (RGBL) of the BESSY II synchrotron radiation facility (HZB Berlin). For further ARPES studies, the sample was transferred from RGBL in argon atmosphere. For the ARPES study of pure graphene we used the RGBL-2 photoemission station at the UE-112 PGM-1 beamline at BESSY II. The synthesis procedure was developed at the Resource Center "Physical Methods of Surface Investigation" (RC PMSI) of the Research park of Saint Petersburg State University. The ARPES measurements of B-graphene and the STM studies were performed there as well.

Theoretical calculations of the scanned-energy mode photoelectron diffraction of graphene and B-graphene have been carried out using the EDAC code in the approximation of multiple scattering of electrons.[30] Model clusters describing graphene and B-graphene films on Co(0001) contained approximately 600 atoms. Parameters of the PED geometry such as linear polarization of photons, analyzer acceptance angle of ±9°, normal emission angle, and so forth were used in accordance with the experiment. The similarity of the experimental and theoretical photoelectron energy distribution curves for the C 1s peaks was evaluated using the divergence R-factor.[31]

The DFT calculations of the electronic structure and C 1s core level shifts of pure graphene/Co(0001) were performed within the local spin density approximation (LSDA) to the exchange-correlation (XC) potential in the Perdew−Wang version (PW92)[32] as implemented in the FPLO-14.00-48 code (improved version of the original FPLO code by K. Koepernik and H. Eschrig;[33] http://www.FPLO.de/). The system was modeled using a 16-layer-thick Co film with graphene on both sides. The four outer atomic layers were relaxed until the forces on each atom were less than 5×10^{-3} eV/Å. The relaxation was performed using the generalized gradient approximation (GGA) to the XC potential in the Perdew−Burke−Ernzerhof version.[34] A k-point grid of $12 \times 12 \times 1$ was used to sample the Brillouin zone. The core level shifts in B-graphene/Co were estimated in the (4×4) superstructure with 5 Co layers and a single B atom in the unit cell. Positions of C and Co atoms were taken from the calculation of pure graphene/Co, while the B atom position was relaxed.

The B-graphene/Co(0001) electronic structure calculations were carried out within the GGA approximation in the revised Perdew−Burke−Ernzerhof version (PBEsol).[35] The equilibrium position of a single B atom in graphene/Co(0001) was determined using the projector augmented-wave method[36] as implemented in the VASP code.[37,38] In these calculations, B-graphene/Co(0001) was simulated by a (3×3) in-plane supercell and a 5-layer-thick Co slab, whose surface was covered with a single B-graphene layer lying in the top-fcc registry. The energy cutoff for the plane-wave expansion of wave functions was set to 400 eV and a k-point grid of $3 \times 3 \times 1$ was used to sample the two-dimensional Brillouin zone. The five topmost atomic layers of the system (including B-graphene) were relaxed until the forces on each atom were less than 10^{-2} eV/Å.

The bandstructure calculations of freestanding B-graphene were performed using the Korringa−Kohn−Rostoker method within the atomic sphere approximation to the crystal potential.[39−41] We took an angular momentum cutoff of $l_{max} = 3$ for the Green's function and a k-point mesh of $31 \times 31 \times 1$ for the two-dimensional Brillouin zone integration. Substitutional B−C disorder was treated within the coherent potential approximation (CPA).[42]

■ ASSOCIATED CONTENT

Supporting Information

The Supporting Information is available free of charge on the ACS Publications website at DOI: 10.1021/acs.nanolett.6b01795.

Additional STM results are presented.(PDF)

■ AUTHOR INFORMATION

Corresponding Author

*E-mail: dmitry.usachov@spbu.ru.

Notes

The authors declare no competing financial interest.

DOI: 10.1021/acs.nanolett.6b01795
Nano Lett. 2016, 16, 4535−4543

■ ACKNOWLEDGMENTS

The authors acknowledge the support of Saint Petersburg State University (research Grant 15.61.202.2015) and BMBF (Grant 05K12OD3). I.I.O., M.V.K., L.V.Ya. and D.Yu.U. acknowledge RFBR (Grant 16-29-06410). M.M.O. and E.V.C. acknowledge the support by the Basque Departamento de Educacion, UPV/EHU (Grant IT-756-13), Spanish Ministerio de Economia y Competitividad (MINECO Grant FIS2013-48286-C2-2-P), and Tomsk State University Academic D. I. Mendeleev Fund Program in 2015 (research Grant 8.1.05.2015). We also acknowledge Helmholtz Zentrum Berlin für Materialien und Energie for support within the bilateral Russian-German Laboratory program. We cordially thank Professor V. I. Bregadze for consultations on the boron organic chemistry and the provision of carborane. The work of E.Yu.K. was supported by the German-Russian Interdisciplinary Science Center (G-RISC) funded by the German Federal Foreign Office via the German Academic Exchange Service (DAAD).

■ REFERENCES

(1) Banszerus, L.; Schmitz, M.; Engels, S.; Dauber, J.; Oellers, M.; Haupt, F.; Watanabe, K.; Taniguchi, T.; Beschoten, B.; Stampfer, C. *Sci. Adv.* **2015**, *1*, e1500222.
(2) Novoselov, K. S.; Geim, A. K.; Morozov, S. V.; Jiang, D.; Zhang, Y.; Dubonos, S. V.; Grigorieva, I. V.; Firsov, A. A. *Science* **2004**, *306*, 666−668.
(3) Petrone, N.; Chari, T.; Meric, I.; Wang, L.; Shepard, K. L.; Hone, J. *ACS Nano* **2015**, *9*, 8953−8959.
(4) Haberer, D.; et al. *Phys. Status Solidi B* **2011**, *248*, 2639−2643.
(5) Mao, H. Y.; Lu, Y. H.; Lin, J. D.; Zhong, S.; Wee, A. T. S.; Chen, W. *Prog. Surf. Sci.* **2013**, *88*, 132−159.
(6) Shen, H.; Shi, Y.; Wang, X. *Synth. Met.* **2015**, *210*, 109−122.
(7) Xia, F.; Farmer, D. B.; Lin, Y.-m.; Avouris, P. *Nano Lett.* **2010**, *10*, 715−718.
(8) Lawlor, J. A.; Ferreira, M. S. *Beilstein J. Nanotechnol.* **2014**, *5*, 1210−1217.
(9) Lherbier, A.; Botello-Méndez, A. R.; Charlier, J.-C. *Nano Lett.* **2013**, *13*, 1446−1450.
(10) Pereira, V. M.; Lopes dos Santos, J. M. B.; Castro Neto, A. H. *Phys. Rev. B: Condens. Matter Mater. Phys.* **2008**, *77*, 115109.
(11) Zabet-Khosousi, A.; Zhao, L.; Pálová, L.; Hybertsen, M. S.; Reichman, D. R.; Pasupathy, A. N.; Flynn, G. W. *J. Am. Chem. Soc.* **2014**, *136*, 1391−1397.
(12) Lawlor, J. A.; Gorman, P. D.; Power, S. R.; Bezerra, C. G.; Ferreira, M. S. *Carbon* **2014**, *77*, 645−650.
(13) Zhao, L.; Levendorf, M.; Goncher, S.; Schiros, T.; Pálová, L.; Zabet-Khosousi, A.; Rim, K. T.; Gutiérrez, C.; Nordlund, D.; Jaye, C.; Hybertsen, M.; Reichman, D.; Flynn, G. W.; Park, J.; Pasupathy, A. N. *Nano Lett.* **2013**, *13*, 4659−4665.
(14) Usachov, D. Y.; Fedorov, A. V.; Petukhov, A. E.; Vilkov, O. Y.; Rybkin, A. G.; Otrokov, M. M.; Arnau, A.; Chulkov, E. V.; Yashina, L. V.; Farjam, M.; Adamchuk, V. K.; Senkovskiy, B. V.; Laubschat, C.; Vyalikh, D. V. *ACS Nano* **2015**, *9*, 7314−7322.
(15) Rosei, R.; De Crescenzi, M.; Sette, F.; Quaresima, C.; Savoia, A.; Perfetti, P. *Phys. Rev. B: Condens. Matter Mater. Phys.* **1983**, *28*, 1161−1164.
(16) Gamo, Y.; Nagashima, A.; Wakabayashi, M.; Terai, M.; Oshima, C. *Surf. Sci.* **1997**, *374*, 61−64.
(17) Kawanowa, H.; Ozawa, H.; Yazaki, T.; Gotoh, Y.; Souda, R. *Jpn. J. Appl. Phys.* **2002**, *41*, 6149.
(18) Parreiras, D. E.; Soares, E. A.; Abreu, G. J. P.; Bueno, T. E. P.; Fernandes, W. P.; de Carvalho, V. E.; Carara, S. S.; Chacham, H.; Paniago, R. *Phys. Rev. B: Condens. Matter Mater. Phys.* **2014**, *90*, 155454.
(19) Bianchini, F.; Patera, L. L.; Peressi, M.; Africh, C.; Comelli, G. *J. Phys. Chem. Lett.* **2014**, *5*, 467−473.
(20) Zhang, W.-B.; Chen, C.; Tang, P.-Y. *J. Chem. Phys.* **2014**, *141*, 044708.
(21) Varykhalov, A.; Rader, O. *Phys. Rev. B: Condens. Matter Mater. Phys.* **2009**, *80*, 035437.
(22) Varykhalov, A.; Marchenko, D.; Sánchez-Barriga, J.; Scholz, M. R.; Verberck, B.; Trauzettel, B.; Wehling, T. O.; Carbone, C.; Rader, O. *Phys. Rev. X* **2012**, *2*, 041017.
(23) Pacilé, D.; Lisi, S.; Di Bernardo, I.; Papagno, M.; Ferrari, L.; Pisarra, M.; Caputo, M.; Mahatha, S. K.; Sheverdyaeva, P. M.; Moras, P.; Lacovig, P.; Lizzit, S.; Baraldi, A.; Betti, M. G.; Carbone, C. *Phys. Rev. B: Condens. Matter Mater. Phys.* **2014**, *90*, 195446.
(24) Usachov, D.; Fedorov, A.; Otrokov, M. M.; Chikina, A.; Vilkov, O.; Petukhov, A.; Rybkin, A. G.; Koroteev, Y. M.; Chulkov, E. V.; Adamchuk, V. K.; Grüneis, A.; Laubschat, C.; Vyalikh, D. V. *Nano Lett.* **2015**, *15*, 2396−2401.
(25) Preobrajenski, A. B.; Ng, M. L.; Vinogradov, A. S.; Mårtensson, N. *Phys. Rev. B: Condens. Matter Mater. Phys.* **2008**, *78*, 073401.
(26) Giovannetti, G.; Khomyakov, P. A.; Brocks, G.; Karpan, V. M.; van den Brink, J.; Kelly, P. J. *Phys. Rev. Lett.* **2008**, *101*, 026803.
(27) Gebhardt, J.; Koch, R. J.; Zhao, W.; Höfert, O.; Gotterbarm, K.; Mammadov, S.; Papp, C.; Görling, A.; Steinrück, H.-P.; Seyller, T. *Phys. Rev. B: Condens. Matter Mater. Phys.* **2013**, *87*, 155437.
(28) Gao, L.; Ren, W.; Xu, H.; Jin, L.; Wang, Z.; Ma, T.; Ma, L.-P.; Zhang, Z.; Fu, Q.; Peng, L.-M.; Bao, X.; Cheng, H.-M. *Nat. Commun.* **2012**, *3*, 699.
(29) Grüneis, A.; Kummer, K.; Vyalikh, D. V. *New J. Phys.* **2009**, *11*, 073050.
(30) García de Abajo, F. J.; Van Hove, M. A.; Fadley, C. S. *Phys. Rev. B: Condens. Matter Mater. Phys.* **2001**, *63*, 075404.
(31) Saiki, R.; Kaduwela, A.; Sagurton, M.; Osterwalder, J.; Friedman, D.; Fadley, C.; Brundle, C. *Surf. Sci.* **1993**, *282*, 33−61.
(32) Perdew, J. P.; Wang, Y. *Phys. Rev. B: Condens. Matter Mater. Phys.* **1992**, *45*, 13244−13249.
(33) Koepernik, K.; Eschrig, H. *Phys. Rev. B: Condens. Matter Mater. Phys.* **1999**, *59*, 1743−1757.
(34) Perdew, J. P.; Burke, K.; Ernzerhof, M. *Phys. Rev. Lett.* **1996**, *77*, 3865−3868.
(35) Perdew, J. P.; Ruzsinszky, A.; Csonka, G. I.; Vydrov, O. A.; Scuseria, G. E.; Constantin, L. A.; Zhou, X.; Burke, K. *Phys. Rev. Lett.* **2008**, *100*, 136406.
(36) Blöchl, P. E. *Phys. Rev. B: Condens. Matter Mater. Phys.* **1994**, *50*, 17953−17979.
(37) Kresse, G.; Furthmüller, J. *Phys. Rev. B: Condens. Matter Mater. Phys.* **1996**, *54*, 11169−11186.
(38) Kresse, G.; Joubert, D. *Phys. Rev. B: Condens. Matter Mater. Phys.* **1999**, *59*, 1758−1775.
(39) Korringa, J. *Physica* **1947**, *13*, 392−400.
(40) Kohn, W.; Rostoker, N. *Phys. Rev.* **1954**, *94*, 1111−1120.
(41) Lüders, M.; Ernst, A.; Temmerman, W. M.; Szotek, Z.; Durham, P. J. *J. Phys.: Condens. Matter* **2001**, *13*, 8587.
(42) Gyorffy, B. L. *Phys. Rev. B* **1972**, *5*, 2382−2384.

DOI: 10.1021/acs.nanolett.6b01795
Nano Lett. 2016, 16, 4535−4543